Polarisation in Photon Absorption Experiments

Alexander Natter and Peter Grabmayr

Physikalisches Institut, Tübingen University

for the A2 Collaboration, Mainz

Production of polarized photons

Polarization and asymmetry measurements play an increasingly important role in medium energy physics as they have provided a large amount of recent progress.

Linearly polarized photons can be produced on a crystal by coherent bremsstrahlung. The regular structure of atoms within a coherence volume leads to an enhancement of radiation of polarized photons within a finite phase space. The cross section for production of bremsstrahlung on a crystal (cr) is composed of a coherent (co) and a incoherent (in) part

$$\sigma^{cr} = \sigma^{co} + \sigma^{in} = \sigma_\perp + \sigma_\parallel + \sigma^{in},$$

where σ is used as an abbreviation for the differential cross section. The incoherent cross section differential in photon energy k has a smooth $1/k$ energy dependence while the coherent cross section exhibits structures related to the periodicities of the lattice (see Figs. 1,2). The coherent part can be decomposed into two contributions, whose photon polarization vector is perpendicular ($\perp$) or parallel ($\parallel$) to the orientation of a reference plane defined by the incoming electron and the lowest reciprocal lattice vector of the crystal. Their difference determine the photon beam polarization P:

$$P = \sigma^{dif}/\sigma^{cr} = (\sigma_\perp - \sigma_\parallel)/\sigma^{cr} = \frac{\sigma_\perp - \sigma_\parallel}{\sigma_\perp + \sigma_\parallel}\left(1 - \frac{1}{R}\right),$$

where $R = \sigma^{cr}/\sigma^{in}$. Based on the work by Timm [1] and the Göttingen group [2] we have improved the description of the incoherent as well as the coherent processes by use of (i) more recent realistic form factors and a realistic angular distribution and (ii) a more detailed description of the beam divergence, collimator function and multiple scattering within thick radiators.

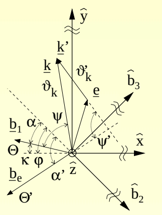

Figure 1: Definition of vectors and angles within the reciprocal lattice.

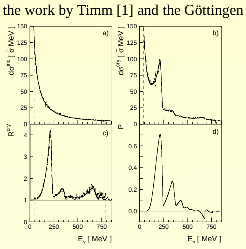

Figure 2: Comparison of measured and calculated spectra. a) Ni radiator b) diamond radiator, c) ratio of diamond/nickel yield d) predicted polarisation.

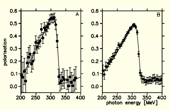

Figure 3: Comparison of measured and calculated polarisation.

This work [4, 5] produced two codes, one relies on the Monte-Carlo technique for a most precise calculation of all effects and a second one for quick surveys where some analytical expressions replaced the time consuming integrations. The accurate description of the photon polarisation from a ^{4}He($\vec{\gamma}$,π°) experiment (see Fig. 3 from ref. [2]) as well as the photon energy spectra for amorphous and crystalline radiators (see Fig. 2) gives the confidence for further predictions. Fig. 2 shows a comparison of electron spectra obtained at $E_\circ$=855 MeV on nickel and diamond radiators with our Monte Carlo predictions.

References

[1] U. Timm, Fortschritte der Physik **17** (1969) 765

[2] F. Rambo *et al.*, Phys. Rev. **C58** (1998) 489

[3] H. Bilokon *et al.*, Nucl. Instr. Methods **204** (1983) 299

[4] A. Natter, contrib. paper to 4^{th}Workshop on electromagnetically induced Two-Hadron Emission, Granada 1999, ISBN: 84-699-1645-9

[5] A. Natter *et al.*, Nucl. Instr. Methods, to be published http://www.pit.physik.uni-tuebingen.de/grabmayr/software/software.html

Linearly polarized photons at low energies

Systematic investigations at various electron energies demonstrated that a better selection of single lattice vectors can be achieved at higher electron energies than for lower ones (compare Figs. 1, 2 and 3). This fact originates from the very low transversal momentum transfer and the principal scaling proportionality of of $E_\circ/a$, where $E_\circ$ is the electron energy and a specifies the basic lattice cell.

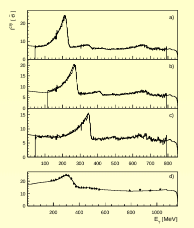

Figure 1: Calculated intensity spectra for diamond crystals at 3 settings at MAMI B and at TAGX (1.2 GeV).

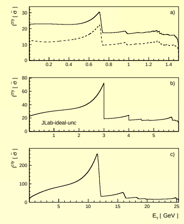

Figure 2: Coherent intensity spectra calculated for electron energies available at various accelerators. a) MAMI C @ 1.5 GeV, b) Jlab @ 4 GeV, c) ELFE @ 27 GeV

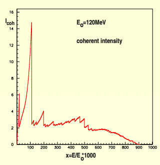

Figure 3: Calculated coherent intensity for $E_\circ$=120 MeV. No beam divergence and straggling in radiator is considered.

In contrast to the single structures in the coherent contributions at high energies one observes for a low energetic electron beam (see Fig. 3) a wealth of lattice vectors which satisfy the Laue condition. There are no crystals with significant smaller lattice cells available. For remedy we suggest to use thick crystals (100 μm) and moderate beam divergences (ε= 0.1 mrad$\times$0.5 mm). Both measures smear out the wealth of structures but still produce significant polarisation.

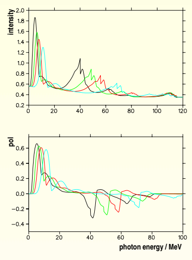

Figure 4: Four different crystal settings covering the low photon energy part.

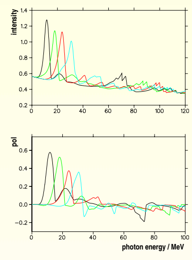

Figure 5: Four different crystal settings covering the high photon energy part.

Fig. 4 demonstrates for S-DALINAC energies (E_o=120 MeV) that the photon range up to E_γ=35 MeV can be covered by four angular settings of the diamond using the [02$\bar{2}$] lattice vector. The figure show the total intensity in the top panel and the polarisation in the bottom one; the four settings are colour coded. For the energy range 35<E_γ<60 MeV the [04$\bar{4}$] vector provides about 30% polarisation, sufficiently large for experiments (Fig. 5).

Polarization in the ^{4}He($\vec{\gamma}$,np) reaction

The studies of the two-nucleon knockout reaction aim at the understanding of short range nuclear force, i.e. nucleon-nucleon correlations in atomic nuclei. The np channel is sensitive also to the tensor part whereas the pp channels tests the central part only. Due to the transverse character of real photons the competing process of meson-exchange currents contribute strongly; isobaric currents and final-state interaction produce additional background contributions some of which are separated kinematically.

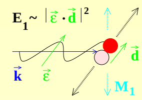

Figure 1: Schematic sketch of the photon interacting with the np pair.

Polarization degrees of freedom are assumed [1] to be less affected by the competing processes. From Fig. 1 one expects negative polarization of the (γ,np) process at intermediate energies where the **M1**-character prevails. Multiple scattering or pion production leading to two detected nucleons will exhibit no polarisation.

Amongst other light nuclei ^{4}He has been chosen for its special features of (i) sitting at the border line between the few-body systems and 'real nuclei' (as defined by the universal behaviour of the total photoabsorption cross sections) and of (ii) being less affected by FSI than heavier nuclei studied sofar.

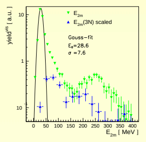

Figure 2: Comparison of two-body missing mass spectra (green) with that for ppn-triples detected.

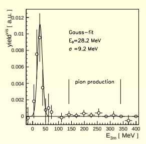

Figure 3: Three-body missing mass E_{3m} showing a sharp peak at threshold.

The experimental setup of the PiP/ToF experiments at the Glasgow tagger facility of the MAMI accelerator is described elsewhere (e.g. [2, 3]). The reconstructed missing energy E_{2m} for two-nucleon emission - which is a measure of the excitation of the residual - is shown on logarithmic scale in Fig. 2(green). One notices the huge peak of the two-body breakup at E_{2m}=28 MeV followed by a tail extending to E_{2m}=170 MeV and a second structure around 250 MeV due to pion production. With small probability also ppn triple are recorded in the detector setup; their distribution (blue) does not show this low-E_{2m} peak. However, plotting the 3-particle missing energy E_{3m} (Fig. 3) yields a sharp peak again, demonstrating that indeed the tail region of the E_{2m} distribution origins due to relative energy in the residual np system.

The determined asymmetries support the interpretation of sizeable negative polarisation for low missing energies (Fig. 4). The photon energy dependence of the yield for E_{2m} <50 MeV (Fig. 5) is different from that for ^{12}C and for D. The change of slope between 200 and 300 MeV was predicted by J. Ryckebusch [4] and is supposedly due to tensor correlation, which must be verified be a more detailed calculation. Finally, the asymmetry for the 3-particle reaction (Fig. 6) is slightly positive; clearly different from that for two-body breakup.

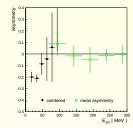

Figure 4: Asymmetry of missing energy (E_{2m}) in the photon range 170-400 MeV.

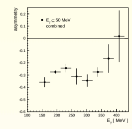

Figure 5: Asymmetry of the ^{4}He($\vec{\gamma}$,np) reaction for E_{2m} <50 MeV.

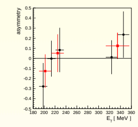

Figure 6: Asymmetry of the ^{4}He($\vec{\gamma}$,npp) reaction.

References

[1] S. Boffi *et al.*, Nucl. Phys. **A564** (1983) 473

[2] P. Grabmayr, Prog. Part. Nucl. Phys. **44** (2000) 113

[3] F.A. Natter, Prog. Part. Nucl. Phys. **44** (2000) 461

[4] J. Ryckebusch, priv. comm